FLOW DISTURBANCES GENERATED BY FEEDING AND SWIMMING ZOOPLANKTON

Thomas Kiørboe[1], Houshuo Jiang[2], Rodrigo J. Gonçalves[1,3], Lasse Tor Nielsen[1], Navish Wadhwa[4]

[1]Centre for Ocean Life, DTU Aqua, Technical University of Denmark, Kavalergården 6, 2920 Charlottenlund, Denmark;

[2]Department of Applied Ocean Physics & Engineering, Woods Hole Oceanographic Institution, Woods Hole, MA 02543, USA.

[3]Estación de Fotobiología Playa Unión (Casilla de Correo 15, 9103 Rawson, Chubut, Argentina)

[4]Centre for Ocean Life, Department of Physics, Technical University of Denmark, DK-2800 Kgs. Lyngby, Denmark

Classification:

Biological Sciences; *Ecology*

Physical Sciences; *Applied Physical Sciences*

Interactions between planktonic organisms, such as detection of prey, predators, and mates, are often mediated by fluid signals. Consequently, many plankton predators perceive their prey from the fluid disturbances that it generates when it feeds and swims. Zooplankton should therefore seek to minimize the fluid disturbance that they produce. By means of particle image velocimetry, we describe the fluid disturbances produced by feeding and swimming in zooplankton with diverse propulsion mechanisms, and ranging from 10-µm flagellates to > mm-sized copepods. We show that zooplankton, in which feeding and swimming are separate processes, produce flow disturbances during swimming with a much faster spatial attenuation (velocity u varies with distance r as $u \propto r^{-3}$ to r^{-4}), than that produced by zooplankton for which feeding and propulsion are the same process ($u \propto r^{-1}$ to r^{-2}). As a result, the spatial extension of the fluid disturbance produced by swimmers is an order of magnitude smaller than that produced by feeders at similar Reynolds numbers. The 'quiet' propulsion of swimmers is achieved either through swimming erratically by short-lasting power-strokes, generating viscous vortex rings, or by 'breast stroke swimming'. Both produce rapidly attenuating flows. The more 'noisy' swimming of those that are constrained by a need to simultaneously feed is due to constantly beating flagella or appendages that are positioned either anteriorly or posteriorly on the (cell) body. These patterns transcend differences in size and taxonomy and have thus evolved multiple times, suggesting a strong selective pressure to minimize predation risk.

Keywords: predation risk; biological fluid dynamics; optimization;

Significance

Plankton compromise their survival when they swim and feed because the fluid disturbances that they generate may be perceived by predators. Since the abundance and population dynamics of zooplankton in the ocean is governed by their access to food and exposure to predators, an important question is to what extent and how zooplankton may minimize the fluid disturbances that they generate. We show that when swimming and feeding are integrated processes, zooplankton generate fluid disturbances that extend much further in the water than is the case for zooplankton that swim only to relocate. Quiet swimming is achieved through 'breast swimming' or by swimming-by-jumping, while other propulsion modes are much noisier. This pattern applies independent of organism size and species.

\body

Zooplankters move to feed, find food, and find mates, so moving is critical to the efficient execution of essential functions. However, moving comes at a predation risk: Swimming increases the predator encounter velocity (encounter rate increases with prey velocity to a power ≤ 1), and feeding and swimming generate fluid disturbances that may be perceived by rheotactic predators, thus increasing the predator's detection distance (encounter rate increases with detection distance squared) (1-5). So, the advantages of moving and feeding must be traded off against the associated risks, and organisms should aim at moving and foraging in ways that reduce the predation risk and optimize the tradeoff (6, 7). They may do so by moving in patterns that minimize encounter rates (8) and/or they may feed and propel themselves in ways that generate only small fluid disturbances (9). For example, theoretical models suggest that zooplankton that swim by a sequence of jumps may create a smaller fluid disturbance than a similar sized one that swims smoothly (9), that a hovering zooplankter generates a larger fluid signal than one that cruises through the water (10, 11), and that a zooplankter moving at low Reynolds numbers will generate a relatively larger fluid signal than one moving at higher Reynolds numbers (11). Thus, motility patterns and propulsion modes may strongly influence predation risk and must be subject to strong selection pressure during evolution.

Zooplankton span a huge taxonomic diversity and a large size range (microns to centimeters) and their propulsion mechanisms vary substantially (12). Unicellular plankton may use one or more flagella or cilia, and the flagella may be smooth or plumose, which has implications for whether the cell is pulled or pushed by the beating flagellum (13). Ciliates may have the cilia rather evenly distributed on the cell surface, or concentrated on certain parts of the cell, typically either anteriorly or as an equatorial band. Small animals may have an anterior 'corona' of cilia (e.g., rotifers and many pelagic invertebrate larvae) to generate feeding currents and propulsion, or they may have

beating or vibrating appendages that can be positioned anteriorly, ventrally, or laterally. The implications and potential adaptive value of this diversity of propulsion modes for feeding and survival are largely unexplored.

Various idealized models, simplifying the swimming organisms to combinations of point forces acting on the water, have been used to describe the fluid disturbance generated by moving and feeding plankton. A self-propelled plankton is often described by a so-called stresslet (two oppositely directed point forces of equal magnitude), a hovering one by a stokeslet (a stationary point force), and a jumping animal by an impulsive stresslet (a stresslet working impulsively) (9, 11, 12). These highly idealized models yield very different predictions of the spatial attenuation of the fluid disturbance and, thus, of how far away the feeding and swimming animal can be detected. A few studies have compared observed flow patterns with those predicted from these simple models and in some cases found fair comparisons (4, 14-17). However, numerical simulations as well as observations of self-propelled microplankton have demonstrated that the distribution of propulsion forces, i.e., the position of flagella, cilia, or appendages on the (cell) body may have a profound effect on the imposed fluid flow (18, 19). Also, most of the idealized models ignore the fact that swimming in most cases is unsteady, which leads to fluctuating flows at scales smaller than the Stokes length scale ($\sqrt{\nu/\omega}$, where ν is the kinematic viscosity and ω is the beat frequency) (e.g. 19). The simple, idealized models hitherto applied may be insufficient to represent the diverse propulsion modes observed in real organisms and to understand the associated tradeoffs.

Feeding and swimming are often part of the same process in zooplankton. Many zooplankton generate a feeding current that at the same time propels the animal through the water. In others, feeding and swimming are separate processes. For example, ambush feeding ‘sit-and-wait’ zooplankters do not move as part of feeding but may swim in order to undertake vertical migration,

or to search for mates or patches of elevated food availability. Also, many of the plankton that generate a feeding current by vibrating appendages may in addition swim by using the same appendages in a different way (e.g., the nauplius larvae of most crustaceans), or by using other swimming appendages dedicated to propel themselves (most pelagic copepods and cladocerans).

While feeding and swimming may both compromise the survival of the organism, the tradeoffs may be different. To get sufficient food, zooplankters need to daily clear a volume of water for prey that corresponds to about 10^6 times their own body volume (20, 21) and hence, implicit in the feeding process is the need to examine or process large volumes of water. In contrast, dedicated swimming should translate the organism through the water as quietly as possible. Thus, we hypothesize that in microplankton, dedicated swimming produces flow fields that attenuate more readily and/or have a smaller spatial extension than the cases in which feeding and propulsion are intimately related.

In this study we use Particle Image Velocimetry (PIV) to describe the flow fields generated by micron to mm sized feeding and swimming zooplankton that use a variety of propulsion modes. We show that – across taxa and sizes – dedicated swimming produces flow fields with a much smaller spatial extension and faster spatial attenuation than those produced by the plankton for which feeding and swimming are integrated, and we characterize the propulsion modes that minimize susceptibility to rheotactic predators.

Results

The propulsion modes vary substantially between the organisms studied here, in terms of the nature of the propulsion machinery (flagella, cilia, appendages), the location of the propelling structure on the organism (anteriorly, posteriorly, ventrally, laterally), in the frequency and duration of the power strokes, and in the resulting speed and variability in speed (Fig. 1, 2, Table S1 and Movie

S1). These different ways of propelling the organism result in a fascinating diversity of flow fields (Fig. 3, Movie S2-4).

The dinoflagellates (20-50 µm) all swim by beating two flagella, a longitudinal, trailing flagellum that propels the cell through the water, and a transverse flagellum that accounts for rotation and steering of the cell (22). The beating of the trailing flagellum creates a succession of short-lasting, counterrotating vorticity structures in the wake of the cell (Fig. 3a) and a highly fluctuating extension of the flow field (Fig. 2a). The rotifer *Brachionus plicatilis* (25-50 µm) generates a feeding current and is pulled through the water by cilia organized in frontal 'coronas' that propel constantly (Movie S1); the resulting propulsion speed is near constant (Table S1) and the flow field is almost stationary in time and consists of two vortex rings, one around the translating body and another one of opposite direction around the feeding current (Movie S2). The nauplius (larval stage) of the copepod *Temora longicornis* (200-300 µm) creates very different flow fields depending on whether it vibrates its 3 pairs of appendages to generate a feeding current, or it swims by a powerful backward strokes of the appendages (Movie S3). The latter flow field is similar to that produced by the swimming nauplii of the copepod *Acartia tonsa* (140-240 µm) as well as by the ciliate *Mesodinium rubrum* (25 µm) and the much larger cladoceran, *Podon intermedius* (0.7-1.0 mm): The flow both anterior and posterior to the organism is in swimming direction, while the flow lateral to the organism is directed backwards (Fig. 3 and Movies S2-3). These organisms all 'breast stroke swim' by beating the laterally positioned appendages or cirri backwards. The copepodites of the three calanoid copepods all swim and feed by vibrating the anterior-ventrally positioned 5 pairs of feeding appendages in a rhythmic but convoluted pattern, but the flow fields differ depending on whether the animal is 'hovering', i.e., generates a feeding current while itself remaining stationary and tethered by gravity (*Temora longicornis*, 0.75 mm), or is cruising through the water (*Metridia longa*, 2.5 mm) (Fig. 3c,e). The third calanoid copepod, *Acartia tonsa* (0.8 mm) is intermediate

between the other two in that it simultaneously swims through the water and generates a feeding current (Movie S4), but it also differs in that it vibrates both its feeding appendages and its swimming legs when generating the current and propelling itself (Movie S1). Finally, all the copepods can swim by sequentially kicking the 4-5 pairs of ventrally positioned swimming legs backwards, either once or a few times (a repositioning jump; *Acartia tonsa*; *Oithona davisae* females), repeatedly at a high frequency (escape jump, none analysed), or repeatedly at a lower frequency (swimming by jumping; *Oithona davisae* males). In all cases, and best illustrated by *Acartia tonsa* (Fig. 3b, Movie S4), two ephemeral vortex rings form, one in the wake of the animal, and one around its forward moving body. A simple categorization of the swimming and feeding behaviors described above is presented in Table 1.

Ignoring details in the flow structures and focusing on how bulk induced flow velocity attenuates with distance to the organism, striking patterns emerges (Fig. 4, Table 1, Table S1). For most species the imposed flow velocity is variable in time. The temporal variation in flow velocity is highest for small organisms and very near the body of the organisms, while at distances approaching or exceeding the Stokes length scale, the flow field is more constant in time. As a consequence, the spatial attenuation of the flow field is variable (Fig.4). However, in the far field, and at the peak of the power stroke, the spatial attenuation tends towards a constant power relationship that is characteristic for each of the flow fields examined and robust to whether the organisms is viewed from the dorsal, ventral, or lateral side (Fig. 4, Table S1). For the zooplankton that swim independent of feeding, the spatial attenuation of the flow is fast, and attenuates with distance to power near -4 for the ones that move by jumps (all the copepods) and near -3 for those that have the swimming appendages organized laterally (the copepod nauplii, *Podon intermedius*, *Mesodinium rubrum*). For those organisms and propulsion modes where swimming and feeding are intimately associated, the spatial attenuation is slower, with powers of between -2 and -1. The

copepodite of *Acartia tonsa* deviates from this pattern in that its feeding current attenuates rapidly. The flow attenuation is related to, but not well predicted by, the Reynolds number of the moving organism (Fig. 2e) and organisms moving at the highest Reynolds numbers (Re > 10) show almost the full range of spatial attenuations. Thus, the propulsion mode is more relevant than the magnitude of Re for the imposed flow pattern.

As a consequence of the differences in spatial attenuation, the spatial extensions of the flow fields differ (Fig. 2d). Here, we define the spatial extension of the flow field, *S*, as the peak cross sectional area within which the imposed fluid velocity exceeds a certain threshold velocity. We have chosen a critical velocity of 0.5 mm s^{-1}: this overlaps with or is close to the highest velocities produced by the smallest organisms examined and the lowest velocities measurable for the largest organisms. In case of no overlap, we extrapolated from observations using the estimated power of the spatial attenuation. The resulting area of course depends on the chosen threshold, but the pattern is robust to the choice of threshold: the area of the flow field increases with the Reynolds number of the organism, and is nearly an order of magnitude larger for plankton that feed and swim simultaneously compared to those where feeding and swimming are separate processes. In organisms for which we have recordings of both feeding and pure swimming modes, e.g. nauplii of *T. longicornis* and copepodites of *A, tonsa,* one can see that they can increase their peak propulsion speed by more than one order of magnitude without (*A. tonsa*) or by only slightly (factor 2.3; *T. longicornis*) increasing the spatial extension of the flow field, as defined above (Fig. 4; Table S1).

Discussion

Our observations suggest that for plankton that swim to relocate, propulsion has been optimized to minimize the fluid disturbance that they generate, whereas for plankton in which swimming is

constrained by a simultaneous need to feed, the fluid disturbance generated is many-fold higher with a consequently higher risk of being detected by a rheotactic predator. Because rheotactic predators respond to imposed fluid velocity magnitude rather than shear (23), the area of influence can be thought of as the encounter cross section towards a rheotactic predator, and thus scales directly with predator encounter rate. The threshold velocity of 0.5 mm s^{-1} was chosen for practical reasons (see above) and a threshold on the order of 0.1 mm s^{-1} would be more in line with typical threshold flow velocities for prey detection in planktonic predators (21), and such a threshold yields an even larger difference between swimmers and feeders. The higher risk associated with feeding than with pure swimming, of course, may be warranted by the benefits of feeding, and thus plankton is no different from many other organisms that have to compromise their survival to acquire food (6).

What are the characteristics of ‘quiet’ propulsion in contrast to ‘noisy’ feeding and swimming and how do the swimmers reduce the spatial extension of their fluid disturbance? The propulsion speed in almost all the organisms examined is unsteady due to the beating of appendages or flagella but the size-dependent beat frequencies do not differ significantly between the swimmers and feeders (Table S1). However, the power strokes are shorter in pure swimmers, their peak speeds as well as variability in speed is much larger than in similar sized feeders, and their propulsion consequently much more erratic (Fig. 2c,Table S1, Movie S1). The higher Reynolds numbers of the swimmers than those of equal sized feeders can only partly account for the limited extension of their flow fields. We have previously shown for swimming plankton that if the power stroke is short relative to the Stokes time scale, the flow structure formed may be characterized by two viscous vortex rings with a fast spatial and temporal attenuation (9). All the jumping and swimming copepods in fact produce two such vortex rings (Fig. 3, Movie S2-4) consistent with previous observations in different species (4, 17, 24), and the observed far field spatial attenuation of the flow ($u \sim r^{-4}$) is

consistent with that predicted from the idealized impulsive stresslet model (Table 1). Thus, the rapid power strokes may be considered an adaptation to minimize the production of fluid signals.

None of the other swimmers examined, the ciliate (*M. rubrum*), the copepod nauplii (*A. tonsa, T. longicornis*), and the cladoceran (*P. intermedius*) form similar vortex rings, but they are all 'breast swimmers' with the propulsion apparatus positioned (bi)laterally symmetrically (Fig. 1, Movie S1), and with quite similar flow fields (Movie S2-S4). The far field flow generated by them all resembles that of a potential dipole (Appendix SI). A potential dipole can physically be thought of as a fluid point sink and a fluid point source, with strengths of equal magnitude *m*, to be placed at two points separated by a distance δ in such a way that $m \times \delta$ remains constant when the separation δ vanishes (25). A potential dipole is mathematically equivalent to a magnetic dipole. The striking swimming appendages follow rather well the streamlines of a potential dipole (equivalent to the magnetic field lines) (Appendix SI, Movie S5), which explains the similarities of the flows. Bulk properties of the flows are also similar in that the observed far field flow attenuation for these swimmers are close to that predicted by the dipole ($u \sim r^{-3}$) and the flow fields, streamlines, and velocity magnitudes are well predicted by the dipole model (Appendix SI). A previous computational fluid dynamics simulation study of the ciliate *Mesodinium rubrum* has similarly shown a dipole-like flow pattern and $\sim r^{-3}$ flow attenuation (26). 'Breast swimming' can thus be considered an adaptation to minimize the fluid disturbances of swimming plankton. Its existence over a large size range and in diverse taxa suggests that this body plan and propulsion mode has evolved multiple times in the course of evolution. Note that the nauplius is the characteristic pelagic larva not only of copepods but of many crustaceans, an abundant and widespread animal group in the ocean, and the nauplius has been characterized as one of the most successful larval forms in the pelagic environment larvae (27).

The zooplankton that feed and swim simultaneously either cruise through the water (*M. longa*, the dinoflagellates), they hover in an almost stationary position while producing a feeding current (*T. longicornis* copepodite), or they do something in between, i.e., translating through the water and simultaneously drawing water towards themselves (all the others). With the exception of *A. tonsa* copepodites, their observed far field spatial attenuation of the flow fields scales with the distance to powers between -1 and -2, comparable to that predicted by the idealized stokeslet (hovering, -1) and stresslet (cruising, -2) models (See Appendix SI).

There is an additional consistent taxa-transcending difference between swimmers and feeders that allow the swimmers to further reduce their susceptibility to rheotactic predators: The swimmers swim intermittently, while the feeders feed and swim almost continuously – a difference that applies generally and not only to the study organisms. The frequency of reposition jumps in copepods and the ciliate is between 1.0-0.01 s^{-1} (28, 29, reviewed in 4) with each jump lasting only a few milliseconds. The males of the copepod *Oithona* spp. swim for only about 1/3 of their time (30) and the actual swimming takes up only a fraction of that time. The cladoceran similarly have long breaks between swimming events. In contrast, flagellates, most ciliates, rotifers, nauplii and copepods that generate a feeding current or cruise while feeding do so almost continuously (10, 28, 31). Because the swimmers propel faster than the feeders, the total distance they cover per unit time, and hence the average predator encounter velocity, may not be different between swimmers and feeders, but the swimmers produce only ephemeral flow structures and are ‘invisible’ to rheotactic predators for most of the time.

The copepod *A. tonsa* is different from the other feeding copepods, in that its flow field attenuates faster than predicted by the idealized models. It also differs in the way it produces the feeding current by vibrating both the feeding and the swimming appendages, as has been observed in other species of the genus (32), and that it feeds only intermittently and for only 5-20 % of the time (33).

This suggests that its feeding current is very efficient and that its exposure to rheotactic predators limited, which in turn may account for the evolutionary success of this particular family, as judged both from its numerical dominance in neritic plankton communities around the world and its capacity to colonize new areas (34-37).

Propulsion strategy may be adapted to optimize a variety of functions. Hitherto propulsion and feeding in zooplankton have mainly been examined from the perspective of food acquisition and propulsion energetics (12), but optimization of feeding and propulsion should not only consider the energetics but also take inescapable predation risk into account (3). Our study suggests that predation is a strong selective agent in shaping the motility and propulsion strategy of zooplankton, and that these organisms can substantially reduce their susceptibility to rheotactic predators as they swim when they are not constrained by a simultaneous need to gather food.

Methods

Most experimental organisms were taken from our laboratory cultures. Exceptions were the copepod *Metridia longiremis* that was collected in Disko Bay, Greenland, and the cladoceran *Podon intermedius* that we collected in Gulmar Fjord, Sweden. We used particle image velocimetry (PIV) to visualize 2D transects of the fluid flow generated by swimming plankton. Briefly, swimming and/or feeding zooplankters were filmed with a high resolution (1280 x 800 pixels), high speed (100-2200 frames s^{-1}) Phantom V210 video camera. The camera was equipped with lenses to produce appropriate fields of view (i.e., such that the entire extension of the flow field was covered), between 0.28 x 0.17 mm^2 for the smallest flagellates to 28 x 17 mm^2 for the largest copepods. Copepods (nauplii and copepodites) and cladocerans swam in small aquaria, varying in size between 1 x 1 x 4 cm^3 (nauplii, small copepodidss) and 5 x 5 x 5 cm^3 (small copepods and cladocerans) to 8.5 x 10.2 x 3.2 cm^3 (large copepods). Protists swam in ~ 0.5 mm high, 10 mm

radius chambers mounted on a microscopic slide. In all cases the fluids were seeded with tracer particles to visualize the flow, 0.5 µm polymer microspheres for the protists and 5- 10 µm hollow glass spheres or ~ 1 µm titaniumoxide particles for the larger organisms. Illumination was provided by a pulsed infrared laser (808 nm) that was synchronized with the camera and passed through optics to produce a thin sheet (150 – 300 µm). The camera was oriented perpendicular to the laser sheet. The dinoflagellates, the rotifer, and the copepod nauplii were filmed in an inverted microscope. In this case the depth of the narrow focal plane rather than a laser sheet defined the thickness of the flow structure recorded. We selected short movie sequences (40-500 frames) where the organisms moved in the focal plane or in the plane of the laser sheet. Because the imaging is in 2D and swimming is in 3D, this is a potential source of variation, but we minimized this variation by selecting sequences where the peak estimates of the spatial extension of the flow field (see below) was constant in time (i.e. not increasing or decreasing). These sequences were analyzed using DaVis PIV software to get quantitative descriptions of the temporal variation of the flow field generated by the swimming/feeding organism. We quantified the spatial extension of the flow by measuring the area, $S(U^*)$, within which the induced flow velocity exceeds a threshold value, U^*, for different values of U^*. Velocity estimates were made at a resolution of 16 pixels x 16 pixels, and $S(U^*)$ was estimated as the fraction of squares with velocity estimates exceeding U^* multiplied by the area of the field of view. And we describe the spatial attenuation of the flow by plotting U^* as a function of the equivalent circular radius of that area. We did not mask the organisms prior to extracting the flow fields, and the motion of the organism itself thus appears as induced water motion. The reasons for not masking are two-fold: (i) we focus on the far field flow and hence a correct description of the near field is of less importance, and (ii) by not masking we correctly estimate the area influenced by the organism. For presentation purposes, and to visualize the near field flow, we masked the animals (Fig. 3, Movies S2-S5). We computed the body Reynolds

number of the feeding and swimming organisms as Vl/ν, where V is the peak velocity of the animal relative to the fluid (i.e., its swimming velocity + the oppositely directed component of feeding current velocity, both measured relative to the camera), l is the body length of the organism, and ν is the kinematic viscosity. The swimming speeds of the organisms were obtained by digitizing their position in subsequent frames. We also computed an index of the relative variability in swimming speed, as the peak minus the average speed divided by the length of the organism. To describe the propulsion modes of the different organisms we filmed them in the absence of PIV particles using optimal illumination (Movie S1). We either shone infrared light through the swimming aquarium towards the camera, or we used the light provided by the microscope.

ACKNOWLEDGMENTS. The Centre for Ocean Life is a VKR Center of Excellence funded by the Villum Foundation. The work was further supported by a grant from the Danish Council for Independent Research, Natural Sciences to TK, RJG was supported by CONICET and FONCyT (PICT 2438). HJ was supported by NSF grant OCE-1129496.

References

1. Evans GT (1989) The encounter speed of moving predator and prey. *J Plankton Res* 11: 415–417.
2. Visser AW (2007) Motility of zooplankton: fitness, foraging and predation. *J Plankton Res* 29: 447–461.
3. Gerritsen J, Strickler JR (1977) Encounter probabilities and community structure in zooplankton. Mathematical model. *J Fish Res Bd Can* 34: 73-82.
4. Kiørboe T, Jiang H, Colin SP (2010) Danger of zooplankton feeding: the fluid signal generated by ambush feeding copepods. *Proc R Soc B* 277: 3229–3237.
5. Tiselius P, Jonsson PR, Kaartvedt S, Olsen ME, Jarstad T (1997). Effects of copepod foraging behavior on predation risk: An experimental study of the predatory copepod *Pareuchaeta norvegica* feeding on *Acartia clausi* and *A. tonsa* (Copepoda). *Limnol Oceanogr* 42: 164-170.
6. Houston AI, McNamara JM, Hutchinson JMC (1993) General results concerning the trade-off between gaining energy and avoiding predation. *Phil Trans R Soc Lond B* 341: 375–397.
7. Lima S, Dill LM (1990) Behavioral decisions made under the risk of predation: a review and prospectus. *Can J Zool* 68: 619–640.
8. Visser AW, Kiørboe T (2006) Plankton motility patterns and encounter rates. *Oecologia* 148: 538–546.
9. Jiang H, Kiørboe T (2011) The fluid dynamics of swimming by jumps in copepods. *J Roy Soc Interface* 8: 1090-1103.
10. Tiselius P, Jonsson P 1990. Foraging behavior of 6 calanoid copepods – observations and hydrodynamic analysis. *Mar Ecol Prog Ser* 66: 23-33.

11. Visser AW (2001) Hydromechanical signals in the plankton. *Mar Ecol Prog Ser* 222:1‑24.

12. Guasto JS, Rusconi R, Stocker R (2012) Fluid mechanics of plankton microorganisms. *Ann Rev Fluid Mech* 44: 373-400.

13. Christensen-Dalsgaard KK, Fenchel T (2004) Complex flagellar motions and swimming patterns of the flagellates *Paraphysomonas vestita* and *Pteridomonas danica*. *Protist* 155: 79-87.

14. Catton KB, Webster DR, Brown J, Yen J (2007) Quantitative analysis of tethered and free swimming copepodid flow fields. *J Exp Biol* 210: 299–310.

15. Drescher K, Goldstein RE, Michel N, Polin M, Tuval I (2010). Direct measurement of the flow field around swimming microorganisms. *Phys Rev Lett* 105:168101.

16. Kiørboe T, Jiang H (2013) To eat and not be eaten: Optimal foraging behavior in suspension feeding copepods. *J Roy Soc Interface* 10: 20120693.

17. Murphy DW, Webster DR, Yen J (2012) A high-speed tomographic PIV system for measuring zooplanktonic flow. *Limnol Oceanogr Methods* 10: 1096-1112.

18. Jiang H, Paffenhöfer G-A (2008) Hydrodynamic signal perception by the copepod *Oithona plumifera*. *Mar Ecol Prog Ser* 373: 37-52.

19. Guasto JS, Johnson KA, Gollub JP (2010) Oscillatory flows induced by microorganisms swimming in two dimensions. *Phys Rev Lett* 105:168102.

20. Hansen PJ, Bjørnsen PK, Hansen BW (1997) Zooplankton grazing and growth: Scaling within the 2-2,000-mu m body size range. *Limnol Oceanogr* 42: 35687-704.

21. Kiørboe T (2011) How zooplankton feed: Mechanisms, traits and tradeoffs. *Biol Rev* 86: 311-340.

22. Fenchel T (2001) How dinoflagellates swim. *Protist* 152: 329–338

23. Kiørboe T, Visser AW (1999) Predator and prey perception in copepods due to hydromechanical signals. *Mar Ecol Prog Ser* 179: 81-95.

24. Yen J, Strickler J R (1996) Advertisement and concealment in the plankton: what makes a copepod hydrodynamically conspicuous? *Inv Biol* 115: 191–205.

25. Batchelor GK (1967) *An introduction to fluid dynamics*. Cambridge University Press, Cambridge.

26. Jiang H (2011) Why does the jumping ciliate *Mesodinium rubrum* possess an equatorially located propulsive ciliary belt? *J Plankton Res* 33: 998-1011.

27. Martin JW, Olesen J, Høeg JT (2014) The Nauplius. Pp 8-16 *In*: Martin JW, Olesen J, Høeg JT (Eds): *Atlas of Crustacean Larvae*. John Hopkins University Press, Baltimore.

28. Buskey EJ, Coulter C, Strom S (1993) Locomotory patterns of microzooplankotn: Potential effects on food selectivity of larval fish. *Bull Mar Sci* 53: 29-43

29. Fenchel T, Hansen PJ (2006) Motile behaviour of the bloom-forming ciliate *Mesodinium rubrum*. *Mar Biol Res* 2: 33-40.

30. Kiørboe T (2008) Optimal swimming strategies in mate searching pelagic copepods. *Oecologia* 155:179–192.

31. Titelman J, Kiørboe T (2003) Motility of copepod nauplii and implicatioins for food encounter. *Mar Ecol Prog Ser* 247: 123-135.

32. Rosenberg G (1980) Filmed obsevations of filter-feeding in the marine planktonic copepod *Acartia clausi*. *Limnol Oceanogr* 25: 738-742.

33. Jonsson P, Tiselius P (1990) Feeding behaviour, prey detection and capture efficiency of the copepod *Acartia tonsa* feeding onplanktonic ciliates. *Mar Ecol Prog Ser* 60: 35-44.

34. Durbin EG, Durbin AG, Smayda TJ Verity PG (1983) Food limitation of production by adult Acartia tonsa in Narragansett Bay, Rhode Island. *Limnol Oceanogr* 28: 1199-1213.

35. Hoffmeyer M (2004) Decadal change in zooplankton seasonal succession in the Bahía Blanca estuary, Argentina, following introduction of two zooplankton species. *J Plankton Res* 26: 181-189.

36. David V, Sautour B, Chardy P (2007) Successful colonization of the calanoid copepod *Acartia tonsa* in the oligo-mesohaline area of the Gironde estuary (SW France) – Natural or anthropogenic forcing? *Estuar Coast Shelf Sci* 71: 429-442.

37. Aravena G, Villate F, Uriarte I, Iriarte A, Ibáñez B (2009) Response of *Acartia* populations to environmental variability and effects of invasive congenerics in the estuary of Bilbao, Bay of Biscay. Estuar. *Coast Shelf Sci* 83: 621-628.

Figure legends:

Fig. 1. The study organisms with their diverse propulsion equipment. The dinoflagellate *Oxyrrhis marina* (the other dinoflagellates look similar) (A), the ciliate *Mesodinium rubrum* (B), nauplius of the copepod *Acartia tonsa* (the nauplius of *Temora longicornis* looks very similar) (C), the rotifer *Brachionus plicatilis* (D), the copepod *Oithona davisae* (E), the cladoceran *Podon intermedius* (F), the copepod *Metridia longa* (G), the copepod *Temora longicornis* (H), and the copepod *Acartia tonsa* (I).

Fig. 2: Temporal fluctuations in area of influence, $S_{0.1\ mm/s}$, for the dinoflagellate *O. marina* (A). Peak propulsion speed (B), speed variability index (C) Area of influence, $S_{0.5\ mm/s}$ during the peak of the power stroke (D), and power of spatial flow attenuation (E), all as a function of Reynolds number for swimmers (read symbols and lines) and feeders (blue symbols and lines). The regression lines in (D) are: Swimmers: Log (*S*, mm^2) = -1.54 + 1.36 Log (Re); Feeders: Log (*S*, mm^2) = -0.48 + 1.61 Log(Re). Speed variability index is estimated as the difference between peak and average speed divided by the length of the organism. All data are reported in Table S1.

Fig. 3. Examples of snapshots of flow fields generated by swimming and feeding zooplankton. Swimming *Oxyrrhis marina* (A), nauplius of *Temora longoicornis* producing feeding current (B), swimming *Podon intermedius* (C), cruising *Metridia longa* (D), hovering *Temora longicornis* (E), and repositioning jump of *Acartia tonsa* (F). The position of the organisms is indicated by red ellipses and its swimming direction by white arrows (grey arrow for the hovering *T. longicornis*). Flow field animations for all species examined are show in Movies S2-4.

Fig. 4. Examples of the spatial attenuation of flow velocities. *A. tonsa* copepodit resposiotning jump (A), *O. davisae* female repositioning jump (B), *P. intermedius* swimming (C), *A. tonsa* nauplii swimming (D), *M. longa* cruise-feeding (E), *O. marina* cruise feeding (F), *T. longicornis* nauplius feeding(G), and *T. longicornis* hovering (H). The filled circles show the attenuation at the peak of the power stroke and the open circles the attenuation during the time leading up to the peak at times given in milliseconds. The full lines have slopes between -1 and -4 and were adjusted to line up with the far field flow attenuation at the peak of the power stroke. A characteristic far field flow attenuation was somewhat subjectively assigned to each experiment based on how well it compares with the observations; for observations that were between two integer value, we assigned an intermediate value.

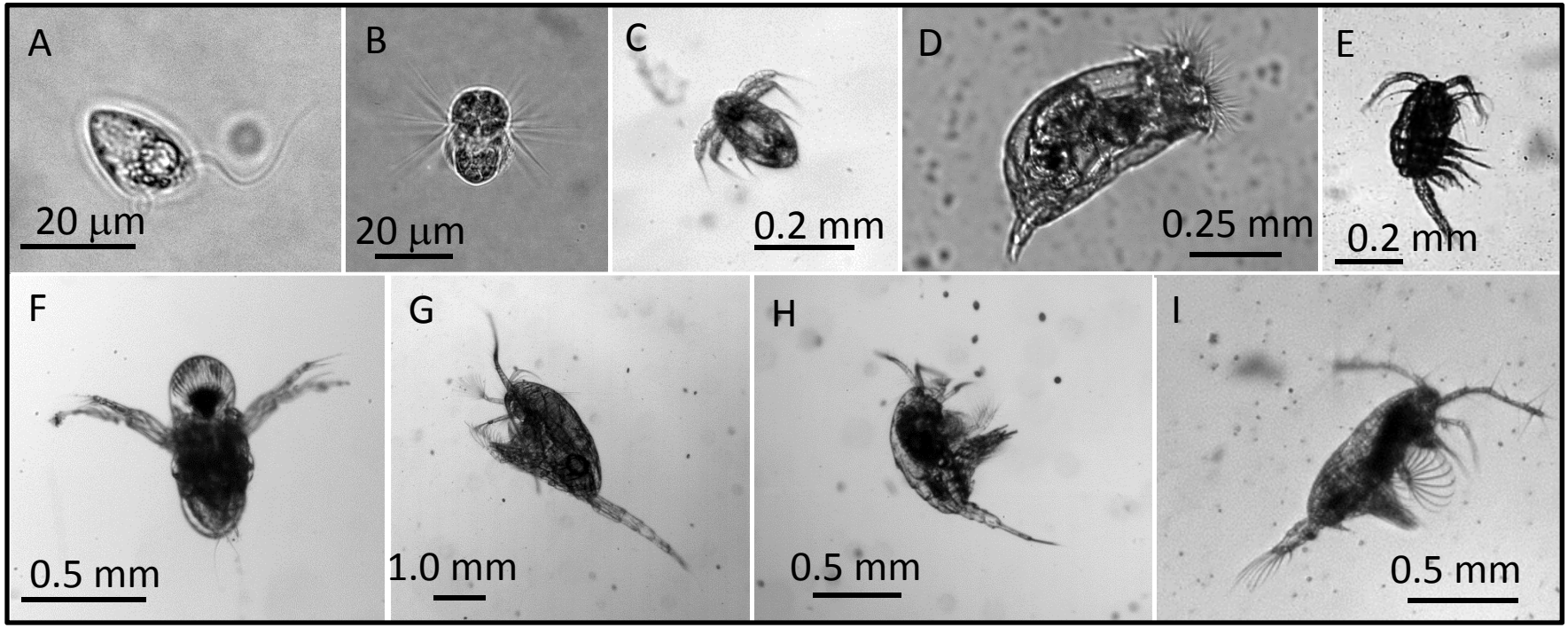
A
20 μm
B
20 μm
C
0.2 mm
D
0.25 mm
E
0.2 mm
F
0.5 mm
G
1.0 mm
H
0.5 mm
I
0.5 mm

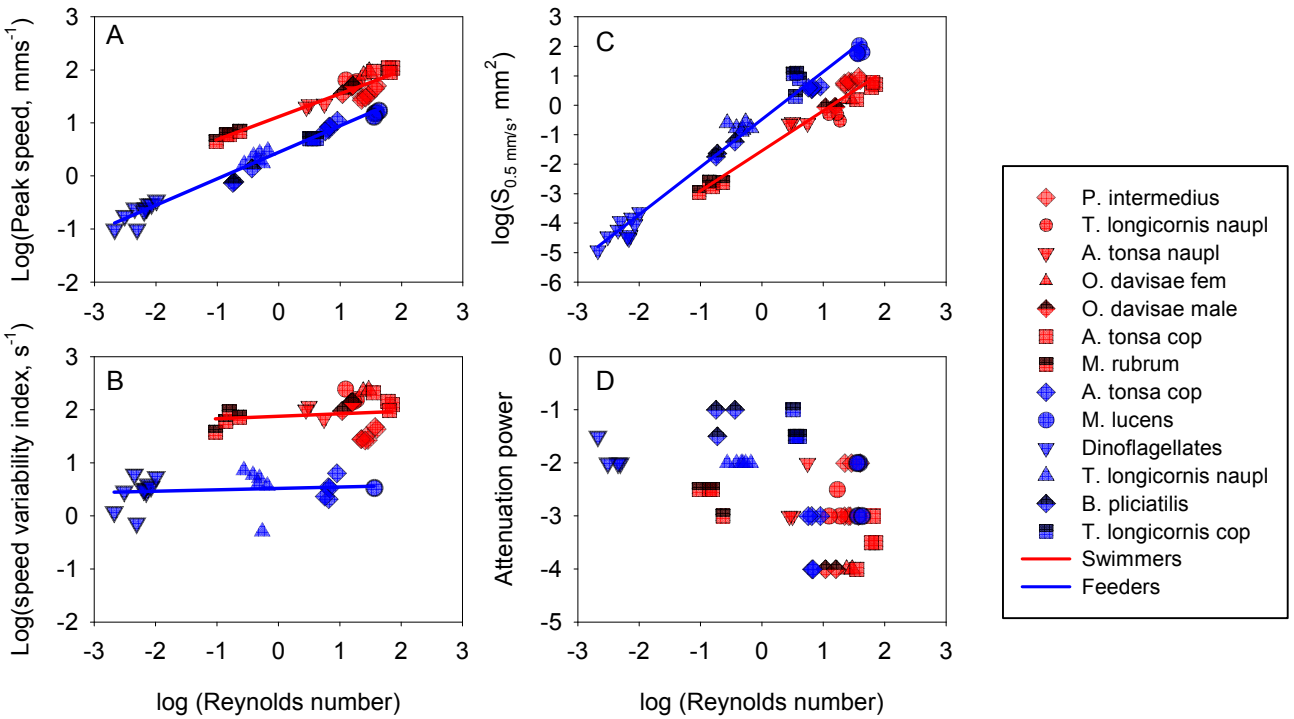
A
B
C
D
Log(Peak speed, mms-1)
Log(speed variability index, s-1)
log(S0.5 mm/s, mm2)
Attenuation power
log (Reynolds number)
log (Reynolds number)
P. intermedius
T. longicornis naupl
A. tonsa naupl
O. davisae fem
O. davisae male
A. tonsa cop
M. rubrum
A. tonsa cop
M. lucens
Dinoflagellates
T. longicornis naupl
B. pliciatilis
T. longicornis cop
Swimmers
Feeders

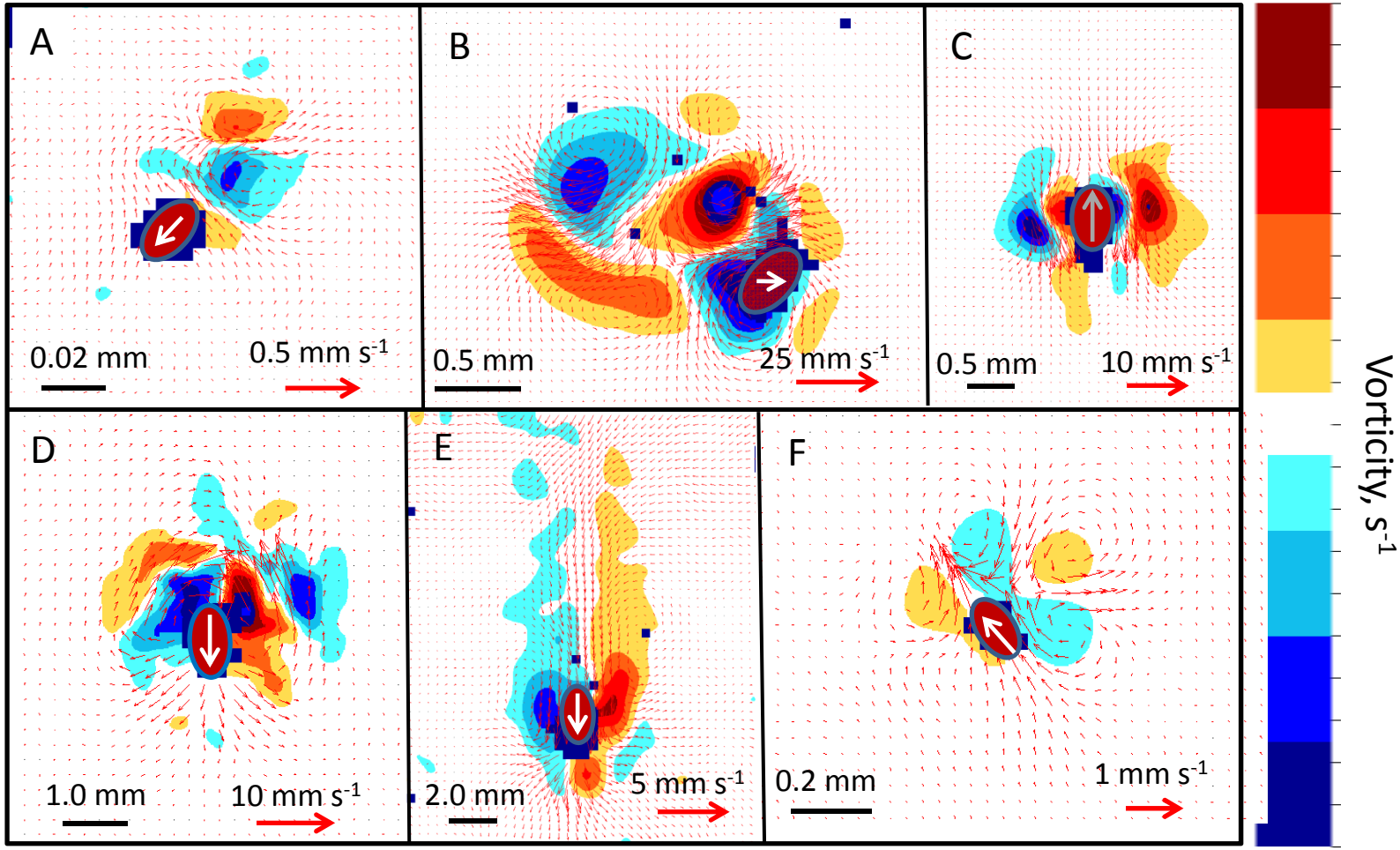
A
0.02 mm
0.5 mm s-1
B
0.5 mm
25 mm s-1
C
0.5 mm
10 mm s-1
D
1.0 mm
10 mm s-1
E
2.0 mm
5 mm s-1
F
0.2 mm
1 mm s-1
Vorticity, s-1

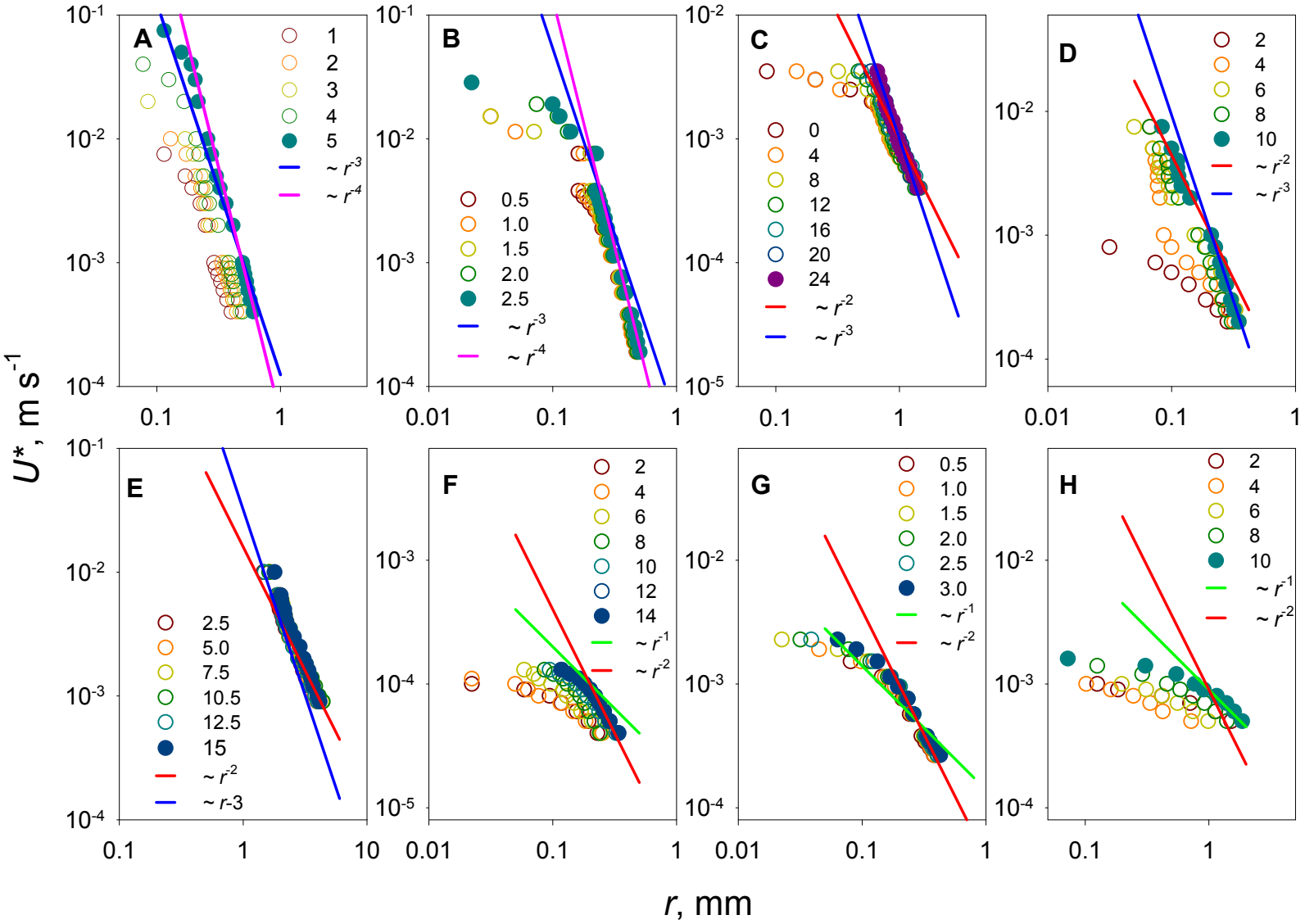
A
1
2
3
4
5
~ r-3
~ r-4
B
0.5
1.0
1.5
2.0
2.5
~ r-3
~ r-4
C
0
4
8
12
16
20
24
~ r-2
~ r-3
D
2
4
6
8
10
~ r-2
~ r-3
E
2.5
5.0
7.5
10.5
12.5
15
~ r-2
~ r-3
F
2
4
6
8
10
12
14
~ r-1
~ r-2
G
0.5
1.0
1.5
2.0
2.5
3.0
~ r-1
~ r-2
H
2
4
6
8
10
~ r-1
~ r-2
U*, m s-1
r, mm

Table 1. Plankton swimming behaviors, their purposes, and bulk properties of the induced flows

Behavior	Purpose	Species/groups	Idealized model	Spatial attenuation[1]
Hover	Feeding	*T. longicornis* copepodite	Stokeslet	r^{-1}
Cruise	Feeding and locomotion	*M. longa*; flagellates	Stresslet	r^{-2}
Hover/cruise	Feeding and locomotion	*B. plicatilis*; *A. tonsa* copepodite feeding; *T. longicornis* nauplii feeding	Stokeslet+Stresslet	r^{-1} to r^{-2}
Breast stroke swim	Locomotion	*M. rubrum*; *P. intermedius*; nauplii swimming	Potential dipole	r^{-3}
Jumping	Locomotion	Copepods swimming by jumping	Impulsive stresslet	r^{-4}

[1]Describes how flow velocity scales with the distance, *r*, from the swimming plankton. The exponent is that predicted from the idealized models (Appendix SI) and approximated by the observations (Table S1, Fig. 4).